Polaron-induced phonon localization and stiffening in rutile TiO_2

Grigory Kolesov
John Paulson School of Engineering and Applied Sciences, Harvard University, Cambridge, Massachusetts 02138, USA

Boris A. Kolesov
Nikolaev Institute of Inorganic Chemistry, SB RAS Novosibirsk, Russia and Novosibirsk State University, Novosibirsk 630090, Russia

Efthimios Kaxiras*
Department of Physics, Harvard University, Cambridge, Massachusetts 02138, USA

(Received 16 December 2016; published 29 November 2017)

Small polaron formation in transition metal oxides, like the prototypical material rutile TiO_2, remains a puzzle and a challenge to simple theoretical treatment. In our combined experimental and theoretical study, we examine this problem using Raman spectroscopy of photoexcited samples and real-time time-dependent density functional theory (RT-TDDFT), which employs Ehrenfest dynamics to couple the electronic and ionic subsystems. We observe experimentally the unexpected stiffening of the A_{1g} phonon mode under UV illumination and provide a theoretical explanation for this effect. Our analysis also reveals a possible reason for the observed anomalous temperature dependence of the Hall mobility. Small polaron formation in rutile TiO_2 is a strongly nonadiabatic process and is adequately described by Ehrenfest dynamics at time scales of polaron formation.

DOI: 10.1103/PhysRevB.96.195165

I. INTRODUCTION

A fundamental unsolved problem in polar materials is how electric charge carriers are generated and how they move through the solid. In these materials electrons deform the highly polarizable crystal lattice and form quasiparticles (polarons) consisting of the electron and a lattice deformation associated with it. In the case of so-called small polarons the strong and complicated electron-lattice interaction renders the usual electronic band-structure description of the charge carriers insufficient. Polarons have also proved important in surface electron transfer processes and photocatalysis on titania where, due to their high binding energy, they act as electron scavengers (Refs. [1–3] and references therein).

Since the 1960s, the availability of high-quality samples and the absence of complex magnetic effects have made rutile titania the prototypical polaron-forming transition metal oxide (TMO). Still, the basic properties of the polaron remain controversial. For instance, reported effective mass values range from 2–150 m_e and room-temperature drift mobility ($\mu_\perp$) values from 0.03–1.4 $cm^2\,V^{-1}\,s^{-1}$ [4–8]. The temperature dependence of mobility also remains the subject of a debate: The drift mobility increases with rising temperature for $T \gtrsim 300$ K, while the Hall mobility decreases. Nonadiabatic polaron theory predicts that both mobilities should rise with temperature due to thermally-activated hopping mechanisms, while adiabatic theory predicts the opposite because of a higher rate of scattering events [5,9–13]. As a possible explanation it was suggested [14] that activation temperature for nonadiabatic hopping is higher in the case of Hall motion, and increase of the Hall mobility should be expected at higher temperatures. However earlier experiments in Ref. [15] where the Hall mobility was shown to decrease within all measured temperature range up to $T = 1250$ K do not agree with this model. Here we report yet another puzzling experimental observation, a phonon-stiffening effect, which is not captured by existing polaron theories that typically predict softening of the phonon modes [11,16–19].

The formation of small polarons in titania was first reported by Bogomolov *et al.* [4,20], who estimated the lower bound of the polaron binding energy to be $\sim$0.4 eV. Recent computations support these findings [21,22], namely that formation of small polarons in rutile titania is energetically favored with a binding energy estimated at $\gtrsim$0.5 eV. The small polaron view has been challenged [6] while other computational studies reported smaller polaron binding energies of $\leqslant$0.15 eV [23,24].

Here we study the properties of polarons in rutile TiO_2 both experimentally and computationally. We use Raman spectroscopy on undoped samples excited with UV laser light. We model the polaron using density functional theory (DFT) and probe the dynamics of its formation with real-time time-dependent density functional theory (RT-TDDFT) which employs mean-field classical-ion (Ehrenfest) dynamics to couple the electronic and ionic subsystems [25]. We show that this approach is adequate to capture the dynamics and time scales of formation of small polarons by photogenerated or injected carriers in rutile TiO_2. In both experiment and theory we observe stiffening of the A_{1g} phonon mode in titania upon UV illumination and upon injection of electrons. The key elements that lead to this effect are the strong electron interactions in d shells of the TM atoms and, closely related to it, the large anharmonic effects of their coupling to the lattice. Based on our results we propose a qualitative model that explains the temperature dependence of the Hall mobility.

II. METHODS

A. Experimental

For the experimental study, we obtained an undoped monocrystalline rutile TiO_2 sample from SurfaceNet GmbH.

*Corresponding author

We measured the Raman spectra using a LabRAM HR Evolution (Horiba) spectrometer with the excitation induced by the 632.8 nm line of a He-Ne laser and the 325.03 nm line of a He-Cd laser. The spectra at room temperature were obtained in the backscattering geometry using a Raman microscope. The diameter of the laser beam spot on the sample surface was around 1–2 μm. The measurements were performed with a spectral resolution of 0.7 cm^{-1} with the 632.8 nm line and 4 cm^{-1} with the 325.03 nm line.

B. Computational

For the theoretical modeling, in both the adiabatic and nonadiabatic (Ehrenfest dynamics) calculations we use our code TDAP-2.0 [25], which is based on the SIESTA package [26,27], an efficient DFT code employing numerical atomic orbitals (NAO) as the basis set. Following Refs. [21,22,28] in this work we use the LDA + U approach in its spherically-averaged form [29], for computational efficiency. In the nonadiabatic part we use TD-DFT and mean-field (Ehrenfest) propagation of classical ions:

$$M_J \frac{\partial^2 \mathbf{R}_J}{\partial t^2} = -\nabla_{\mathbf{R}_J} E_{KS}, \tag{1}$$

where J is the ion index and E_{KS} is the expectation value of electronic energy. The electronic wavefunctions are propagated with effective single-particle TD-DFT equations [30]:

$$i \frac{\partial \phi_n(t)}{\partial t} = \hat{H}_{KS}[\rho](t)\phi_n(t), \tag{2}$$

with ϕ_n being the single-particle Kohn-Sham orbitals, $\hat{H}_{KS}$ the Kohn-Sham effective Hamiltonian operator, and $\rho(\mathbf{r},t) = \sum_{n=1}^{N} |\phi_n(\mathbf{r},t)|^2$ is the electronic density of the system containing N electrons.

To calculate phonon modes and frequencies we used finite atom displacements to construct the dynamical matrix (frozen-phonon method). In all cases described below phonon modes were calculated after complete lattice relaxation with force tolerance 0.02 eV/Å.

C. Simulation setup

We used a $4 \times 4 \times 4$ rutile titania supercell in all our calculations. This cell contains 384 atoms and was found by converging difference between the energies of neutral and charged ($-|q_e|$) supercells to within 0.1 eV (see Table S1 in the Supplemental Material [31]). The Brillouin zone was sampled at the Γ point, except for smaller supercells used in convergence tests where we used Monkhorst-Pack k-point grids starting from $8 \times 8 \times 12$ for a single unit cell. As in the works prior to this [3,25,32], we used PBE + U functional with $U = 4.2$ eV in all our calculations. In this study we used standard SIESTA pseudopotentials and SZP basis set. In all simulations that involved an extra electron or electron-hole pair, we employed a spin-polarized version. In Ehrenfest RT-TDDFT simulations we used a time step $\Delta t = 1$ a.u. ($\approx$24 as). We thermalized the system for 1 ps ($T = 300$ K) with standard BOMD using 1 fs time steps.

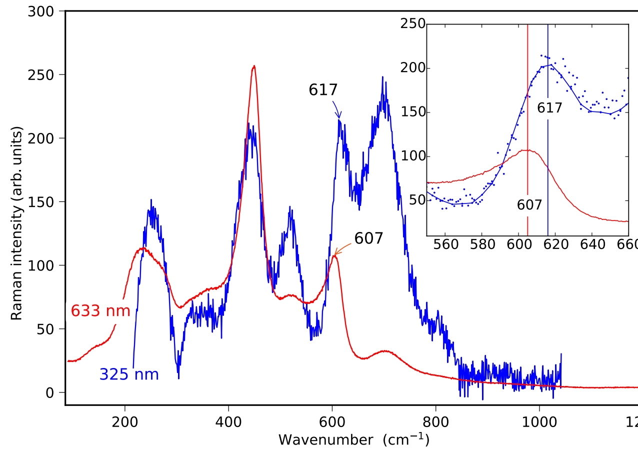

FIG. 1. Raman spectra of rutile titania taken with the 632.8 nm laser (red line) and the 325 nm UV laser (blue line) with $\hbar\omega = 3.8$ eV $> E_{\mathrm{gap}}$. Peak positions in experiment were assigned by deconvolution in Lorentzian functions (see Fig. S1). The inset shows a magnified view of the spectra around the 607 cm^{-1} and 617 cm^{-1} peaks.

III. RESULTS

Rutile TiO_2 has four Raman-active modes with symmetries A_{1g}, E_g, B_{1g}, and B_{2g} [33]. In Fig. 1 we present Raman spectra obtained in the normal state of the sample (red line) and after it was photoexcited with UV laser (blue line). The peaks at 440 and 607 cm^{-1} correspond to the E_g and A_{1g} modes, respectively [33,34], shown schematically in Fig. 2(a). The peak at 143 cm^{-1} (B_{1g} phonon) is obscured by the combination peak at 235 cm^{-1} [33] and cannot be seen in the blue line because it is below the resolution range of the spectrometer used in the UV experiment. The peak at 823 cm^{-1} which corresponds to the B_{2g} mode is known to be exceptionally weak and difficult to resolve [33,34] and is not seen in the spectra presented here. The most interesting feature of the two spectra is a shift of the A_{1g} 607 cm^{-1} peak to the higher wave number of 617 cm^{-1} in the blue spectrum. Typically at higher temperatures of the sample a shift of the peaks to lower wave number is expected [34]. This softening effect is very small for

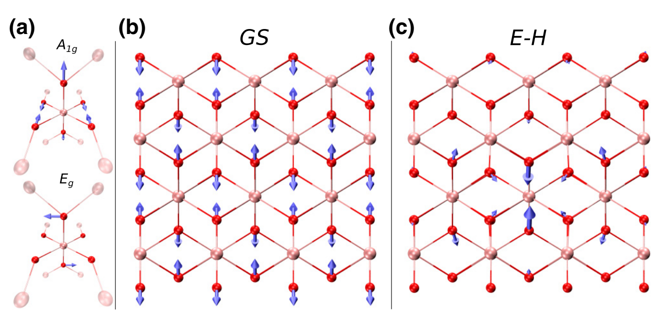

FIG. 2. (a)Stereographic representation of atomic displacements corresponding to the A_{1g} and E_g phonons in the ground state (defect-free) bulk titania. (b) The A_{1g} 607 cm^{-1} phonon displacement in orthographic projection, in the ground state (*GS*) titania. (c) The localized A^*_{1g} phonon at 616 cm^{-1} in the *E-H* simulations (with the corresponding phonon at 611 cm^{-1} in the *E*-simulation being nearly identical, see Fig. S2).

the A_{1g} mode (see Fig. 3 in Ref. [34]). Thus, the shift of the A_{1g} mode to higher wave number cannot be explained by heating of the sample due to carrier relaxation to the band edges, but could be caused by polaron-induced structural changes.

Another interesting feature of the photoexcited sample spectrum is the increase in relative intensity of the sidebands at 520 cm^{-1} and 700 cm^{-1}. There are no zone-center phonons that correspond to these wave numbers. The well-known combination band at 235 cm^{-1} [33], on the contrary, is not observed to have a significant change upon photoexcitation of the sample. Different hypotheses can be put forward to explain the increase of relative intensities of the 520 cm^{-1} and 700 cm^{-1} lines, for instance: (i) the photon energy above the gap energy can lead to indirect resonant process with emission of a $\pm q$ pair of phonons and (ii) processes directly involving polaronic states. In this paper we will focus on the shift of A_{1g} peak as the most striking feature of the spectrum, leaving the change of sideband intensities to a future study.

Our calculation of the lowest charge-neutral excited state within the DFT ΔSCF method [25] yielded excitation energy $E_g^{\Delta\mathrm{SCF}} = 3.7$ eV in the bulk at $T = 0$ K. After correcting this energy for the spin contamination, $E_g \approx 2E_g^{\Delta\mathrm{SCF}} - E_{\mathrm{triplet}}$ [35,36], we obtained $E_g = 3.4$ eV. This agrees very well with the value obtained from BSE calculations (3.3 eV) [37], thus confirming our choice of the value $U = 4.2$ eV, but overestimates the experimental band gap of 3.03 eV. We calculate the polaron binding energy E_p from the difference of total electronic energies of the charged system (with excess charge of $-e$) of the ideal bulk $4 \times 4 \times 4$ supercell and the relaxed supercell with the same charge. Because of the high dielectric constant of titania and large supercell size, we disregarded energy corrections arising from charge interaction between replicas and the compensating uniform positive background charge that is usually introduced to obtain converged energies of charged systems in periodic-cell conditions. This correction is expected to be on the order of 0.1 eV (see Table S1 and Ref. [22], Fig. 1) and is not expected to significantly depend on the value of U [22]. We find $E_p \approx 0.9$ eV. The *lower* bound for E_p in rutile titania was previously estimated from experimental data in the seminal work by Bogomolov *et al.* [4,20] to be ~0.4 eV, and by Austin and Mott [5] to be ~0.6 eV. In both of these works authors suggest that these values are likely to be underestimated. Our value of 0.9 eV is thus in reasonable agreement with these estimates, as well as with values obtained in other $+U$ and hybrid-functional DFT computations [21,22].

To elucidate the origin of the A_{1g} mode stiffening, we calculated vibrational eigenmodes and frequencies using the frozen phonon method. Before performing frozen-phonon calculations in the periodic cell containing an extra electron (to which we refer as the 'E' simulation) and an electron-hole excitation (to which we refer as the 'E-H' simulation), we relax the geometry using a conjugate gradient algorithm, starting from the last point of the corresponding thermalized nonadiabatic trajectories described below. The results for the A_{1g} and E_g modes are presented in Table I.

The agreement between experiment and theory is surprisingly good. Note that for the E_g phonon the experimental peak is expected to redshift with increasing temperature [34], while in the simulation the effect of heating is not included.

TABLE I. Frequencies of A_{1g} and E_g phonons obtained by theory and experiment. *GS* refers to the ground state of titania, while *E* and *E-H* to the extra-electron and photoexcited electron-hole systems.

	A_{1g} frequency (cm^{-1})		E_g frequency (cm^{-1})	
System	Theory	Experiment	Theory	Experiment
GS	603	607	444	449
E	611		444	
E-H	616	617	446	440

Given the limitations of the experimental measurements and of the simulations it could be argued that this surprising level of agreement is due to fortuitous cancellation of errors. Because of the agreement in the *trend*, that is, the stiffening of the A_{1g} mode only, as well as systematic stiffening of this mode with increasing value of U (see Fig. 4 and text below), we suggest that the simulation captures, at least qualitatively, the mechanism of the stiffening, prompting us to analyze further the vibrational and electronic structure of the exciton-polaron system.

In Fig. 2(c) we show the atomic displacement corresponding to the A_{1g} phonon in the E-H simulation (the phonon mode in the E simulation is nearly identical, see Fig. S2). Due to breaking of the crystal symmetry (space group $P\frac{4_2}{m}\frac{2_1}{n}\frac{2}{m}$) by the lattice distortion associated with the polaron, the 616 cm^{-1} phonon in the E-H simulation (and the 611 cm^{-1} in the E simulation) is completely localized around one of the Ti atoms, which we will denote as Ti*. This new phonon is a symmetric oxygen breathing mode which belongs to the A_{1g} representation of the Ti* point group symmetry $\frac{2}{m}\frac{2}{m}\frac{2}{m}$ (D_{2h}). We denote this localized oxygen breathing mode as A_{1g}^* for clarity. One of two degenerate E_g modes (the one involving apical O atoms bonded to Ti* as shown in Fig. 2(a) preserves its character upon formation of the polaron, while the other (at 444 cm^{-1}) wraps around the polaron and does not involve O atoms bonded to Ti* (Fig. S3). We provide an explanation for this effect below. The frequency of both E_g modes is unchanged.

In Fig. 3(a) we show the magnetization density associated with the excited electron (spin-up) and the hole (spin-down). The excited electron is primarily localized on the d_{xy} orbital of the Ti* atom, one of the three nonbonding t_{2g} orbitals [38]. It is partially screened by the hole which is weakly localized on the next-neighbor O atoms. Most of the hole occupies delocalized p-type lone-pair orbitals of the O atoms in the system. The presence of the electron in antibonding states and the hole in bonding states of the system, as well as the mobility of both carriers, should result in an overall softening of the potential. This simple picture ignores the rearrangement of the total electron density caused by the localized electron. In Fig. 3(b) we present the electron density *difference* between the exciton-polaron excited state and the ground state at the same geometry. This plot shows that the localized electron causes further polarization of the Ti*-O bonds with the electron on the e_g-like orbital displaced towards the O atoms. This increase of valence electron density on O atoms compensates for the presence of the hole; indeed, the net Hirshfeld atomic

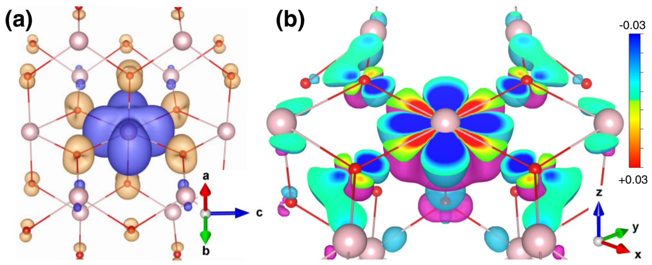

FIG. 3. Electronic structure of the exciton polaron. (a) The magnetization density: blue isosurface represents spin-up (electron) and orange spin-down (hole) magnetization densities. (b) Charge-density difference between the electronic excited and ground states at the same atomic geometry: magenta isosurface represents charge difference (excess of "hole") and cyan negative (excess of "electron") charge difference. We also show the gradient of the density difference on the $(1\bar{1}0)$ cut-through plane, with blue shades depicting excess electron density and red shades depicting excess hole density [see Fig. S4 for a similar picture on the (110) cut-through plane]; the cut-through planes are labeled according to crystallographic directions.

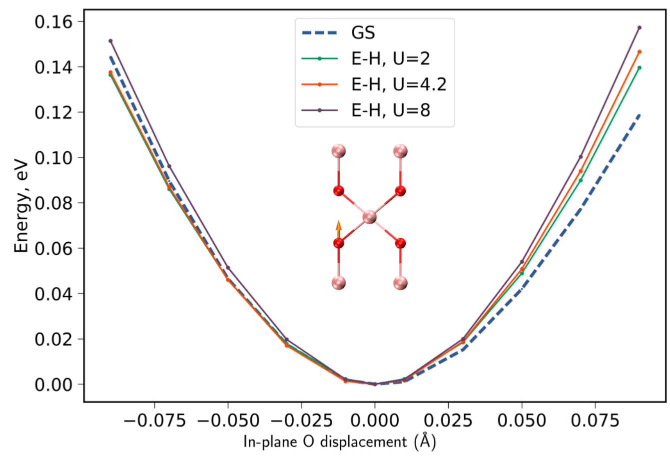

FIG. 4. Total electronic energy as a function of displacement of the O atom along the component of the A_{1g} eigenvector. Green, orange, and purple graphs correspond to the exciton polaron obtained for different values of U and the dashed blue line corresponds to the ground state at the ground state geometry (positive displacement indicates diminished O-Ti*-O angle).

charge on the oxygen atom is the same as in the ground state at the relaxed geometry.

We consider next the displacement of O atoms bonded to Ti* in the $\pm x$, $\mp y$ direction on the $(1\bar{1}0)$ plane, see Fig. 3(b). This corresponds to a scissorlike motion of four in-plane O atoms in the direction of the A_{1g} mode in Figs. 2(a) and 2(b). The inward motion $(-x,+y$ direction for the O atoms in front and $+x,-y$ for the atoms in back) in the excited system should experience a harder potential than in the ground state due to Coulomb repulsion between valence electrons surrounding the O atoms and the excited electron in the lobes of the d_{xy} orbital of the Ti* atom. Alternatively, this can be viewed as hardening due to the action of the Hubbard U with increasing overlap between the bonding p states of O atoms and the d_{xy} orbital of Ti* and the increasing population of the latter state. In rutile titania the oxygen octahedron is distorted and d orbitals belonging to the T_{2g} (reducible) representation are not degenerate; thus the potential cannot be softened by moving the excited electron to another t_{2g} orbital. Outward motion of the O atoms $(+x,-y$ direction for the O atoms in front) is on the contrary softened by the interaction with the excited electron as the atoms move away from it and because of additional Ti-O bond rearrangement. This change in potential leads to almost complete suppression of the scissorlike motion of the four O atoms in the xy plane for the A_{1g}^* phonon, see Fig. 2(b). The effect of Coulomb repulsion is confirmed in Fig. 4, where the potential for the O atom is mapped for different values of U and displays systematic stiffening with increasing U (graphs for $U = 1$ and $U = 6$ in Fig. 4, which conform to the same trend, were left out for clarity). A similar description can be applied to the apical O atoms vibrating along the Ti*-O bond (along the z axis in Fig. 3), with the reduced effect of Coulomb repulsion due to the absence of lobes of the occupied d_{xy} orbital in the z direction (see Fig. S4 and Fig. S5b). The overall effect is stiffening of the potential. Similarly, displacement in the direction of one of the E_g modes, Fig. 2(a), does not change significantly the overlap of O p states and the occupied d_{xy} state of Ti* and thus has a smaller effect on this phonon mode.

The asymmetry of the potential in relation to O motion and Ti* t_{2g} orbitals may have interesting consequences for polaron transport in the presence of a magnetic field. In Fig. 5(a) we show the polaron moving in the c direction. The electron is hopping from the lowest-energy in-plane $d_{||}$ (d_{xy}) orbital of Ti* on the left to the same orbital of the next Ti* on the right. The higher the population of phonon modes that involve in-plane O atoms the higher the rate of nonadiabatic hopping. High population of the phonon modes causes larger displacement for the apical O atoms than for in-plane O atoms, because the potential for the apical O atoms is softer. These large displacements decrease the rate of hopping in the $c_\perp$ direction, because the large displacement of negatively charged apical O atoms leads to increased Coulomb repulsion either by destination orbital $d'_{||}$ $(d_{x'y'}$ orbital in the symmetry-transformed x,y,z coordinates) or by relevant intermediate orbitals belonging to Ti* octahedra, $d_\perp$ (e.g., $d_{xz} + d_{yz}$), through which such hopping must proceed. This effect opposes the Lorentz force that drives the Hall current, see Fig. 5(b). The same argument applies to the motion of the polaron in the $c_\perp$ direction, with the Lorentz force acting in the c direction. The higher the temperature, the higher the population of the polaronic phonon modes, and therefore the higher the drift velocity, the stronger this effect should be. This may explain the observed decrease of the Hall mobility with increasing temperature, while the drift mobility (hopping rate) increases.

IV. FORMATION OF THE POLARON AND EXCITON POLARON

We examined how the polaron is formed in two different simulations. In the first case we introduced a single extra electron into the thermalized ($T = 300$ K) system ('E' simulation). In the second case we introduced an electron-hole (e-h, '$E - H$' simulation) pair by finding the lowest

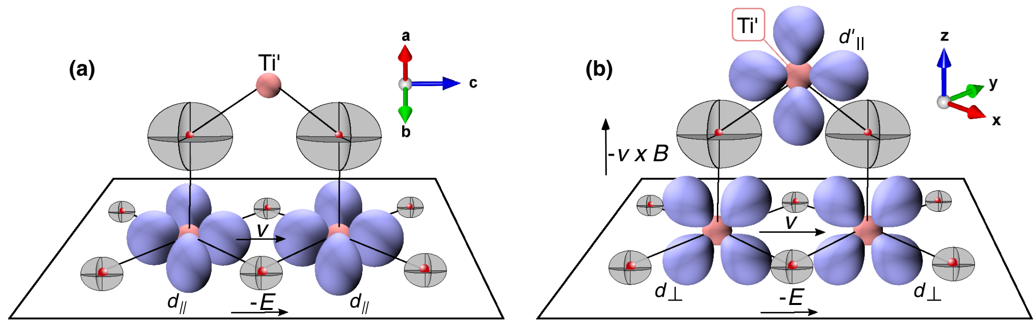

FIG. 5. Scheme of polaron motion in Hall experiment. (a) The polaron is hopping from a Ti* atom on the left to a Ti* atom on the right in the xy plane, with the electron occupying their overlapping in-plane lowest-energy $d_{||}$ (d_{xy}) orbitals. The electric field is in the [00$\bar{1}$] direction. Thermal ellipsoids around the oxygens depict their relative vibrational amplitude. (b) Same as (a) with addition of magnetic field; the Lorentz force acts normal to the plane. The Hall current is directed toward orbital $d'_{||}$ on a Ti′ atom through the intermediate orbitals $d_{\perp}$ on Ti* atoms. The vibrational displacement of apical O atoms shown by ellipsoids elevates the energies of either $d'_{||}$ or $d_{\perp}$ leading to reduced Hall current.

excited state with the ΔSCF method. The *E-H* trajectory is closer to the experimental situation, where e-h pairs are generated by UV light. This choice implicitly assumes that at experimental time scales the majority of the excited electrons relax to the bottom of the conduction band and the holes to the top of the valence band. Prior to introducing the e-h pair we thermalized the system at $T = 300$ K using standard Born-Oppenheimer molecular dynamics (BOMD). To make the comparison between the two simulations more informative, we start both at the same point of the BOMD trajectory, that is, with the same ionic coordinates and velocities. These simulations were performed with Ehrenfest dynamics within RT-TDDFT. As control samples, we used two BOMD trajectories branching from the same original configuration, of which the first corresponded to a neutral ground-state trajectory (*GS* trajectory) and the second to an adiabatic trajectory with an added electron ('$ad - E$'). In both nonadiabatic simulations we observed the formation of a polaron (Fig. 6, Fig. S6, and movie S1). In the *ad-E* simulation, even though we are using the same small time step as in the nonadiabatic simulations (≈24 as), we observed large deviations from energy conservation which lead to divergence of the trajectory in less than 5 fs. This was caused by violation of the conditions of the Born-Oppenheimer approximation: We assume that before the full polaron is formed, there are states with the electron localized on different Ti atoms that are close in energy, while interaction between them is small in comparison to the potential barrier separating them. This confirms that, at least in this case, the formation of the polaron is indeed a nonadiabatic process.

A polaron consists of a localized charge trapped in a self-induced lattice deformation. To quantify the deformation, for each nearest neighbor J of Ti* we compute the quantity κ_J, defined as

$$\kappa_J(t_n) = \sum_{k=1}^{n} \left[d_J(t_k) - d_J^{GS}(t_k)\right]/n, \tag{3}$$

where t_n is the time at time step n, d_J is the distance between Ti* and atom J in the nonadiabatic trajectories (E and E-H), and d_J^{GS} is the same distance in the *GS* BOMD trajectory. We present in Fig. 6 the values of $\kappa_J(t)$ for different species in the neighborhood of Ti*. In both the E and E-H simulations, the deformation converges at roughly 50–60 fs, which matches nicely the 55 fs period of the A_{1g} mode obtained in Raman experiments here and in Ref. [34]. This result is expected from small polaron theory [10,13] and demonstrates that the Ehrenfest approximation captures well the dynamics of small polaron formation. As expected, negatively-charged O atoms are repelled from the Ti* atom in both trajectories and the O-Ti* bond length increases substantially (by ∼0.07 Å).

V. CONCLUSION

Most theoretical polaron models employ a single-particle picture for the electrons and linear electron-phonon interaction terms in order to understand carrier behavior and to interpret experimental results. From such models, softening of the polaron-renormalized phonon frequency $\tilde{\omega}$ is expected, for

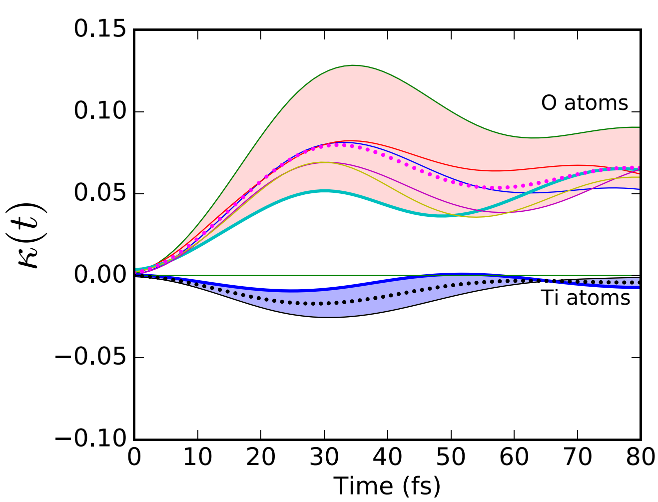

FIG. 6. Lattice distortion associated with formation of the polaron for the photoexcited electron-hole (*E-H*) nonadiabatic trajectory measured in terms of κ Eq. (3), the cumulative average differences from the ground-state-trajectory values of the distances between the Ti* atom and its nearest-neighbor O and Ti atoms. The dotted lines correspond to the average value of κ for each atomic species. (The corresponding plot for the E trajectory is presented in Fig. S6).

any strength of electron-phonon interaction [11,12,16–19]. In contrast to this, we observe stiffening of the A_{1g} mode, both in the experimental Raman spectra and in our DFT simulations. Our analysis of the simulations reveals strong anharmonic effects: Upon breaking of the crystal symmetry by the polaron, the original crystalline A_{1g} mode is transformed into a new oxygen breathing mode which is localized on the polaron. The formation of the polaron is a strongly nonlinear process that involves significant change of the valence electron density around the localized electron. In the simulation, the localization and rearrangement is caused by the Coulomb interaction correction introduced by the Hubbard U term in the DFT + U method. These effects cause overall stiffening and localization of the Raman-active A_{1g} phonon mode. The resulting potential is asymmetric with regard to motion of in-plane and apical oxygens, as well as to t_{2g} and other orbitals in the distorted octahedron. This observation led us to propose a qualitative explanation of the anomalous temperature dependence of the Hall mobility, which decreases with temperature, while the drift mobility increases (above an activation temperature) as expected from nonadiabatic small-polaron theory. The asymmetry of the potential may lead, upon excitation of the phonon modes required for polaron motion in one direction, to higher-amplitude motion of the out-of-plane oxygens, which, through Coulomb repulsion, increase the energy of the orbitals involved in hopping in the direction perpendicular to the drift current, thus reducing the Hall current. As a first step in quantitative modeling of these problems we applied Ehrenfest dynamics with RT-TDDFT to study the formation of the polaron in TiO_2 and demonstrated the usefulness and applicability of this quantum-classical method in describing the dynamics and the timescale of this process. These findings may be relevant to other d and f materials which display small-polaron properties.

ACKNOWLEDGMENTS

This work was supported by an NSF Grant No. EFRI 2-DARE: Quantum Optoelectronics, Magnetolectronics and Plasmonics in 2-Dimensional Materials Heterostructures, Award 1542807. Computational resources were provided by XSEDE [41] (Grant No. TG-DMR120073), which is supported by National Science Foundation Grant No. ACI-1053575, NERSC (ERCAP request number 88881) and the Odyssey cluster, supported by the FAS Research Computing Group at Harvard University.

[1] M. A. Henderson, A surface science perspective on photocatalysis, Surf. Sci. Rep. **66**, 185 (2011).

[2] S. Kuwahara, and K. Katayama, Distinction of electron pathways at titanium oxide/liquid interfaces in photocatalytic processes and co-catalyst effects, Phys. Chem. Chem. Phys. **18**, 25271 (2016).

[3] G. Kolesov, D. Vinichenko, G. A. Tritsaris, C. M. Friend, and E. Kaxiras, Anatomy of the photo-chemical reaction: Excited state dynamics reveals C-H acidity mechanism of methoxy photo-oxidation on titania, J. Phys. Chem. Lett. **6**, 1624 (2015).

[4] V. Bogomolov, E. Kudinov, and Y. A. Firsov, Polaron nature of the current carriers in rutile, Fiz. Tverd. Tela **9**, 3175 (1967).

[5] I. Austin, and N. F. Mott, Polarons in crystalline and non-crystalline materials, Adv. Phys. **18**, 41 (1969).

[6] E. Hendry, F. Wang, J. Shan, T. F. Heinz, and M. Bonn, Electron transport in TiO_2 probed by THz time-domain spectroscopy, Phys. Rev. B **69**, 081101 (2004).

[7] L. Yan, J. E. Elenewski, W. Jiang, and H. Chen, Computational modeling of self-trapped electrons in rutile TiO_2, Phys. Chem. Chem. Phys. **17**, 29949 (2015).

[8] E. Yagi, R. R. Hasiguti, and M. Aono, Electronic conduction above 4 K of slightly reduced oxygen-deficient rutile TiO_{2-x}, Phys. Rev. B **54**, 7945 (1996).

[9] T. Holstein, Studies of polaron motion: Part I. the molecular-crystal model, Ann. Phys. **8**, 325 (1959).

[10] T. Holstein, Studies of polaron motion: Part II. the "small" polaron, Ann. Phys. **8**, 343 (1959).

[11] D. Emin, *Polarons* (Cambridge University Press, New York, 2013).

[12] I. Lang, and Y. A. Firsov, Kinetic theory of semiconductors with low mobility, J. Exp. Theor. Phys. **16**, 1301 (1963).

[13] J. Devreese, Polarons, Encycl. Appl. Phys. **14**, 383 (1996).

[14] A. Alexandrov and N. Mott, *Polarons and Bipolarons* (World Scientific, Singapore, 1995).

[15] I. Bransky, D. Tannhauser, Hall mobility of reduced rutile in the temperature range $300-1250^\circ$ K, Solid State Commun. **7**, 245 (1969).

[16] A. Migdal, Interaction between electrons and lattice vibrations in a normal metal, J. Exp. Theor. Phys. **7**, 996 (1958).

[17] E. Rashba, Teoriya sil'nogo vzaimodeistviya elektronnykh vozbuzhdenii s kolebaniyami reshyotki v molekulyarnykh kristallakh. II, Opt. Spektrosk **2**, 75 (1957).

[18] A. Alexandrov, and H. Capellmann, Phonons in a strongly coupled electron-phonon system, Phys. Rev. B **43**, 2042 (1991).

[19] A. S. Alexandrov, V. V. Kabanov, and D. K. Ray, From electron to small polaron: An exact cluster solution, Phys. Rev. B **49**, 9915 (1994).

[20] V. Bogomolov, and D. Mirlin, Optical absorption by polarons in rutile (TiO_2) single crystals, Phys. Status Solidi (b) **27**, 443 (1968).

[21] N. A. Deskins, R. Rousseau, and M. Dupuis, Localized electronic states from surface hydroxyls and polarons in TiO_2(110), J. Phys. Chem. C **113**, 14583 (2009).

[22] C. Spreafico, and J. VandeVondele, The nature of excess electrons in anatase and rutile from hybrid DFT and RPA, Phys. Chem. Chem. Phys. **16**, 26144 (2014).

[23] M. Setvin, C. Franchini, X. Hao, M. Schmid, A. Janotti, M. Kaltak, C. G. Van de Walle, G. Kresse, and U. Diebold, Direct View at Excess Electrons in TiO_2 Rutile and Anatase, Phys. Rev. Lett. **113**, 086402 (2014).

[24] A. Janotti, C. Franchini, J. Varley, G. Kresse, and C. Van de Walle, Dual behavior of excess electrons in rutile TiO_2, Phys. Status Solidi Rapid Research Letters **7**, 199 (2013).

[25] G. Kolesov, O. Grånäs, R. Hoyt, D. Vinichenko, and E. Kaxiras, Real-time TD-DFT with classical ion dynamics: Methodol-

ogy and applications, J. Chem. Theory Comput. **12**, 466 (2016).

[26] J. M. Soler *et al.* The SIESTA method for *ab initio* order-N materials simulation, J. Phys.: Condens. Matter **14**, 2745 (2002).

[27] S. J. Riikonen, and D. Sánchez-Portal, First principles study of nanostructured surface reconstructions induced by the deposition of metals on vicinal Si(111) surfaces, Ph.D. thesis, Universidad del País Vasco, Spain, 2007.

[28] V. I. Anisimov, M. A. Korotin, J. Zaanen, and O. K. Andersen, Spin Bags, Polarons, and Impurity Potentials in $La_{2-x}Sr_xCuO_4$ from First Principles, Phys. Rev. Lett. **68**, 345 (1992).

[29] S. L. Dudarev, G. A. Botton, S. Y. Savrasov, C. J. Humphreys, and A. P. Sutton, Electron-energy-loss spectra and the structural stability of nickel oxide: An LSDA+U study, Phys. Rev. B **57**, 1505 (1998).

[30] E. Runge, and E. K. U. Gross, Density-Functional Theory for Time-Dependent Systems, Phys. Rev. Lett. **52**, 997 (1984).

[31] See Supplemental Material at http://link.aps.org/supplemental/10.1103/PhysRevB.96.195165 for an additional table, figures, and a movie of the nonadiabatic trajectory.

[32] G. A. Tritsaris, D. Vinichenko, G. Kolesov, C. M. Friend, and E. Kaxiras, Dynamics of the photogenerated hole at the rutile TiO_2(110)/water interface: A non-adiabatic simulation study, J. Phys. Chem. C **118**, 27393 (2014).

[33] S. Porto, P. Fleury, and T. Damen, Raman spectra of TiO_2, MgF_2, ZnF_2, FeF_2, and MnF_2, Phys. Rev. **154**, 522 (1967).

[34] T. Lan, X. Tang, and B. Fultz, Phonon anharmonicity of rutile TiO_2 studied by Raman spectrometry and molecular dynamics simulations, Phys. Rev. B **85**, 094305 (2012).

[35] T. Ziegler, A. Rauk, and E. J. Baerends, On the calculation of multiplet energies by the Hartree-Fock-Slater method, Theor. Chim. Acta **43**, 261 (1977).

[36] T. Kowalczyk, K. Le, and S. Irle, Self-consistent optimization of excited states within density-functional tight-binding, J. Chem. Theory Comput. **12**, 313 (2016).

[37] W. Kang, and M. S. Hybertsen, Quasiparticle and optical properties of rutile and anatase TiO_2, Phys. Rev. B **82**, 085203 (2010).

[38] Here for simplicity we use usual notation applied to octahedral environment. Because in rutile the octahedron is distorted the actual orbital structure and bonding is more complex [39,40].

[39] P. I. Sorantin, and K. Schwarz, Chemical bonding in rutile-type compounds, Inorg. Chem. **31**, 567 (1992).

[40] B. Jiang, J. Zuo, N. Jiang, M. O'Keeffe, and J. Spence, Charge density and chemical bonding in rutile TiO_2, Acta Crystallogr. Sect. A **59**, 341 (2003).

[41] J. Towns, T. Cockerill, M. Dahan, I. Foster, K. Gaither, A. Grimshaw, V. Hazlewood, S. Lathrop, D. Lifka, G. D. Peterson, R. Roskies, J. R. Scott, and N. Wilkens-Diehr, XSEDE: Accelerating scientific discovery, Comput. Sci. Eng. **16**, 62 (2014).